PHOTONICS Research

Independent control of circularly polarized light with exceptional topological phase coding metasurfaces

Yicheng Li,[1,2,3] Shicheng Wan,[1,2,3] Shaoxuan Deng,[1,2] Zhengwei Deng,[1,2] Bo Lv,[1,2] Chunying Guan,[1,2] Jun Yang,[2,4,6] Andrey Bogdanov,[3,5] Pavel Belov,[3] and Jinhui Shi[1,2,*]

[1]Key Laboratory of Photonic Materials and Devices Physics for Oceanic Applications, Ministry of Industry and Information Technology, College of Physics and Optoelectronic Engineering, Harbin Engineering University, Harbin 150001, China
[2]Key Laboratory of In-Fiber Integrated Optics of Ministry of Education, College of Physics and Optoelectronic Engineering, Harbin Engineering University, Harbin 150001, China
[3]School of Physics and Engineering, ITMO University, St. Petersburg 197101, Russia
[4]School of Information Engineering, Guangdong University of Technology, Guangzhou 510008, China
[5]Qingdao Innovation and Development Center, Harbin Engineering University, Qingdao 266000, China
[6]e-mail: yangj@gdut.edu.cn
*Corresponding author: shijinhui@hrbeu.edu.cn

Received 3 November 2023; revised 6 January 2024; accepted 6 January 2024; posted 8 January 2024 (Doc. ID 510300); published 1 March 2024

Exceptional points, as degenerate points of non-Hermitian parity-time symmetric systems, have many unique physical properties. Due to its flexible control of electromagnetic waves, a metasurface is frequently used in the field of nanophotonics. In this work, we developed a parity-time symmetric metasurface and implemented the 2π topological phase surrounding an exceptional point. Compared with Pancharatnam-Berry phase, the topological phase around an exceptional point can achieve independent regulation of several circular polarization beams. We combined the Pancharatnam-Berry phase with the exceptional topological phase and proposed a composite coding metasurface to achieve reflection decoupling of different circular polarizations. This work provides a design idea for polarimetric coding metasurfaces in the future.

https://doi.org/10.1364/PRJ.510300

1. INTRODUCTION

A metasurface, as a two-dimensional artificial material, can achieve unique physical properties by changing the geometric size and periodic arrangement of structural units [1–3]. Metasurfaces offer more compact platforms for the investigation of light-matter interaction, as well as a wide range of practical applications [4,5]. The electromagnetic wave's amplitude, phase, polarization, and nonlinearity could be precisely controlled by the metasurface [6–8], notably the phase modulation, which plays an important role in fields such as metalenses [9], holograms [10], and beam steering [11]. Since its creation, the idea of programmable metasurfaces and digital coding has been extensively researched [12], offering a fresh viewpoint on the real-time control of electromagnetic wave propagation [13–15]. For coding a metasurface, the binary codes "0" and "1," which stand for the discretized reflection phase, have recently been presented as an alternate method of realizing electromagnetic wave manipulation [16–18]. However, the independent control of circularly polarized light based on a phase coding metasurface is still lacking, especially for cross-polarization conversion [16,17]. It is relatively simple to manage linear polarization light by altering the geometric parameters of the metasurface unit structure, while circular polarization (CP) is more challenging. Currently, the mainstream method is to regulate CP through the Pancharatnam-Berry (PB) phase, which has one clear drawback. It is challenging to accomplish independent control of CP light since the phase modulation of the PB phase is the opposite for right-handed circularly polarized (RCP) light and left-handed circularly polarized (LCP) light. Therefore, the composite phase is introduced to achieve multi-dimensional optical field control of multifunctional surface devices [19–21]. The arbitrary phase modification for LCP and RCP light has been accomplished by integrating the propagation phase and PB phase [19]. Even though this approach can produce positive outcomes, an extra simple and straightforward approach is still required to decouple and independently regulate the CP light [21]. Non-Hermitian systems based on parity-time (PT) symmetric transformations have real eigenvalues as well, which were discovered by Bander and Boettcher in 1998 [22]. The exceptional point

(EP), as the phase transition point of open systems, manifests unique characteristics that greatly enrich the research and development in the field of open systems [23–26]. Based on the advantages of flexible construction and the unconstrained regulation of the equivalent permittivity, the research on the non-Hermitian metasurfaces is also highly fascinating, especially in the polarization space [27–31]. There has been a substantial advancement in the fields of chiral detection, polarization imaging, and high sensitivity sensing based on a PT symmetric metasurface. Interestingly, it has been discovered that the surrounding of an EP may produce unique mode selection features and generate a topological phase. This is a new phase formation mechanism to distinguish from the previous propagation phase and PB phase [28]. Exceptional topological phase (ETP) enriches the method of phase regulation and can be combined with traditional phase control, which greatly enriches the design and application of metasurfaces [32–34].

In this work, by designing a PT symmetric metasurface, it is found that the polarization eigenstates have degeneracy at EP, which is related to the chirality of the system, and the 2π-phase accumulation occurs through any path around EP. The independent polarization control of CP light is realized. This novel approach utilizes the phase accumulation generated around the EP, which is plainly distinct from the conventional geometric phase. The potential of phase coding is confirmed based on the ETP, while combined with the conventional PB phase, a composite phase coding metasurface is created to accomplish the independent regulation of RCP and LCP light. This work not only simplifies the structure design and phase distribution of CP regulation but also promotes the development of multifunctional coding metasurfaces.

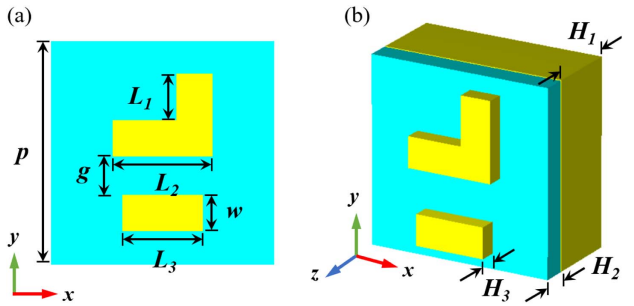

Fig. 1. (a) Schematic of the unit cell of the reflection metasurface composed of two Al structures (yellow) and dielectric layer SiO_2 (blue). $p = 300$ nm, $L_1 = 51$ nm, $L_2 = 140$ nm, $L_3 = 114$ nm, $w = 50$ nm; g denotes the distance between the two structures and $g = 70$ nm. (b) Side view of the metasurface; $H_1 = 150$ nm, $H_2 = 40$ nm, $H_3 = 30$ nm.

2. PRINCIPLE AND DESIGN

As schematically shown in Fig. 1, the metasurface consists of three layers, consisting of two lossy aluminum [35] spaced by silica with permittivity 2.31. The metal background resists all transmission so that the metasurface works in the reflective regime. The structured layer is formed by a chiral structure array and can be excited by x-polarized and y-polarized waves, respectively (see Appendix A). For describing the coupling between two resonators, coupled-mode theory is a popular and efficient method. To create the Hamiltonian matrix for the PT symmetric system, the reflection matrix and coupled-mode equation are combined (see Appendix B). Considering that the reflection matrix $\hat{r}$ and the system Hamiltonian H have the same eigenvector, it is more straightforward to re-express the reflection matrix in the circular polarization basis as [29]

$$\hat{r} = \begin{pmatrix} r_{++} & r_{+-} \\ r_{-+} & r_{--} \end{pmatrix}, \tag{1}$$

where subscripts + and – represent RCP and LCP, respectively. It can be seen from the reflection matrix that $r_{++} = r_{--}$, and the eigenvalues are $r_{1,2} = r_{++} \pm \sqrt{r_{+-}r_{-+}}$. The condition required to achieve EP is $r_{+-}r_{-+} = 0$. Since the x- and y-polarized resonances occur in the metasurface, we can adjust the resonances concerning each other by a variation of the structural parameters, and in consequence, allow for engineering the reflection behavior with $r_{+-} = 0$ or $r_{-+} = 0$, which means EP occurs. Through CST simulation, it can be seen that cross-polarized reflection curve r_{-+} (red curve) suddenly drops nearly to zero at 667 nm in Fig. 2(a), while r_{+-} (blue curve) does not change. This is due to the degeneracy of the eigenpolarization state of the system at the EP, where there is only

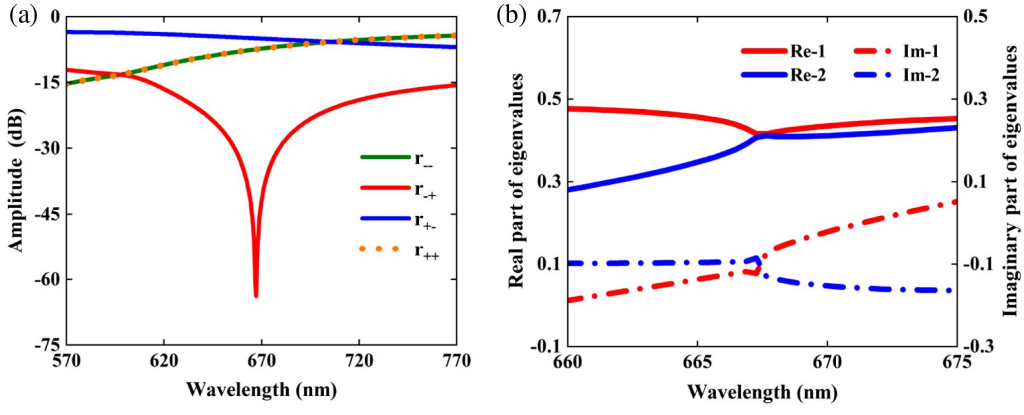

Fig. 2. (a) Spectral dependence of the reflection matrix coefficients. A singularity point, where $r_{-+} = 0$, is observed at $\lambda = 667$ nm. (b) Amplitude and phase of the reflection matrix eigenvalues. Real and imaginary parts of two eigenvalues degenerate at $\lambda = 667$ nm.

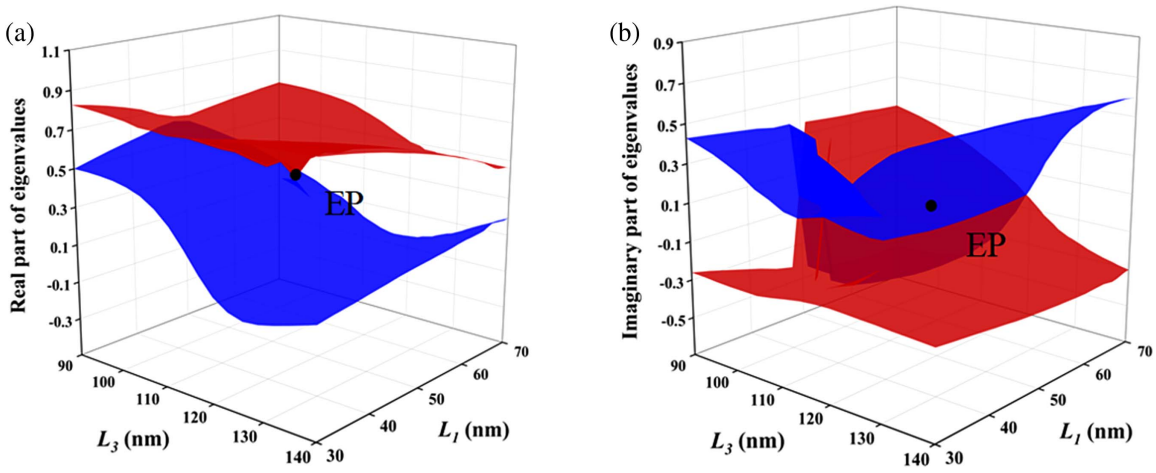

Fig. 3. Simulation results of the metasurface in the parameter space (L_1, L_3). Simulated (a) real and (b) imaginary parts of two eigenvalues at $\lambda = 667$ nm. A self-intersecting Riemann surface profile and EP are observed.

RCP; therefore no cross-polarization conversion r_{-+} occurs. The emergence of EP can be proved more clearly by solving the system eigenvalues. As shown in Fig. 2(b), it is obvious that the real and imaginary parts of the eigenvalues coalesced at 667 nm, which is consistent with the phenomenon in Fig. 2(a).

The degeneracy of eigenvalues is one of the key distinctions between non-Hermitian and Hermitian systems. In a non-Hermitian system, two or more intersecting Riemann surfaces centered around an EP are formed. As shown in Fig. 3, we reveal the evolution of system eigenvalues in parameter space (L_1, L_3). The existence of an EP is demonstrated by the spectrum of r_{-+} and the degeneracy of its eigenvalues and eigenstates at $\lambda = 667$ nm. The intersecting double Riemann surface that corresponds to the eigenvalues of the reflection matrix further supported this pattern. It is very evident that the eigenvalues will be switched rather than the recurrence of their original values under a single full loop around the EP, and they will only do so under two full loops. This provides

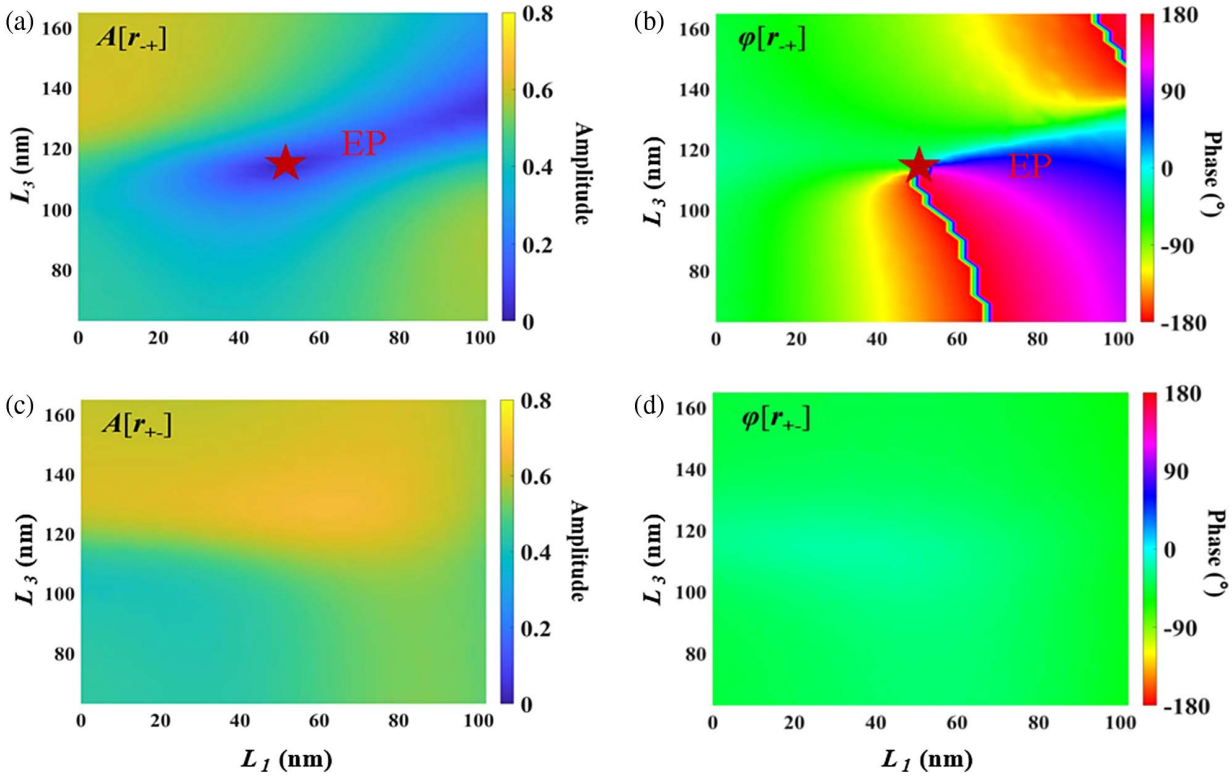

Fig. 4. Amplitude and phase of CP conversion coefficients of the reflection matrix. (a), (b) Amplitude and phase of the structure for RCP incidence. (c), (d) Amplitude and phase of the structure for LCP incidence in the parameter space in the range of $L_1 \in (0, 100)$ (nm) and $L_3 \in (60, 160)$ (nm). An EP appears at $(L_1, L_3) = (51, 114)$ (nm) in cross reflection amplitude r_{-+} and cross reflection phase φ_{-+}.

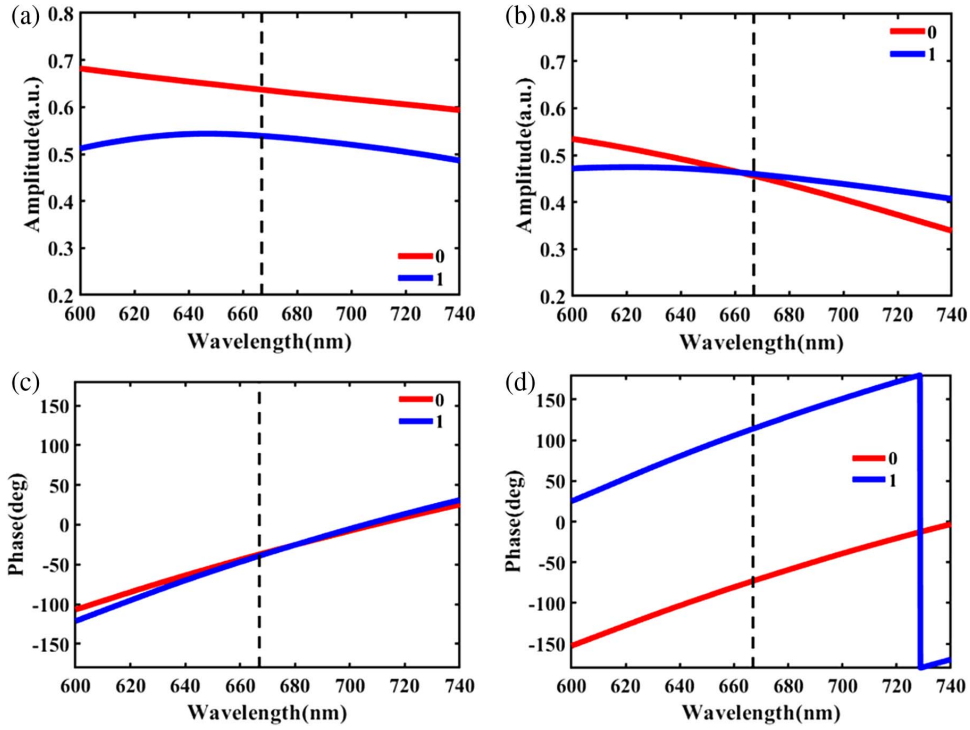

Fig. 5. Amplitude and phase of CP conversion coefficients with "0" (red curve) and "1" (blue curve) elements. (a) Amplitude of CP conversion r_{+-} for LCP incidence, (b) amplitude of CP conversion r_{-+} for RCP incidence, (c) phase φ_{+-} for LCP incidence, and (d) phase φ_{-+} for RCP incidence.

clear and convincing evidence that the EP exists in our system [28,31,36].

To observe the exceptional topologic phase of the eigenvalues' surface, two parameters need to be varied, as shown in Fig. 4. L_1 and L_3 were chosen because they play important roles in the y- and x-polarized resonances [28]. As expected, the reflection matrix from the metasurface can be tailored with varying parameters. By changing the geometric parameters of the structures, it can be clearly seen that EP appears only when a single circular polarization is incident, and there is a significant 2π phase accumulation around EP. As long as the reflected phase encircles one EP in parameter space, the 2π phase accumulation is preserved regardless of the closed path. In contrast to the classical PB phase, this type of phase accumulation caused by circling a singularity exhibits a clear topological robustness.

Compared to the conventional coding metasurface, the ETP metasurfaces require no complicated phase independent CP control [16]. Choosing the "0" and "1" elements, as shown in Fig. 5, the parameters of the two elements are as follows: $(L_1, L_3) = (81, 102)$ (nm) and $(L_1, L_3) = (48, 135)$ (nm). With the RCP, due to the existence of an EP, there is a π phase delay between the two elements, and the reflective amplitudes are almost the same as shown in Figs. 5(b) and 5(d). On the contrary, since there is no EP under the LCP incidence, their phase values are the same. Thus, it is possible to achieve CP coding independently. It is worth noting that both elements "0" and "1" have no phase differences when rotation occurs. This is merely due to differences in geometric parameters, which are also distinct from the conventional use of PB phase for CP encoding.

Since ETP is a topological phase generated around a singularity, it can be combined with PB phase to achieve more complex phase coding (see Appendix C). In Fig. 6, we chose the previous "0" and "1" elements, represented in green and blue, to satisfy the phase delay π for RCP incidence. We implement the new coding unit at LCP incidence by rotating the "0" and "1" elements that exist only at the ETP for RCP incidence,

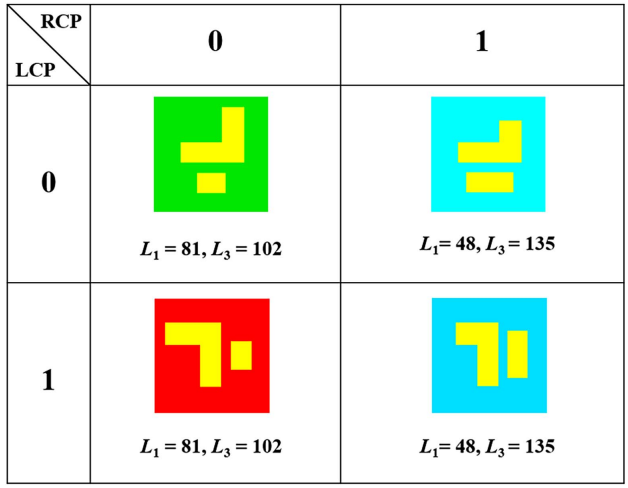

Fig. 6. Structure of the unit cells for the ETP and PB phase coding metasurface.

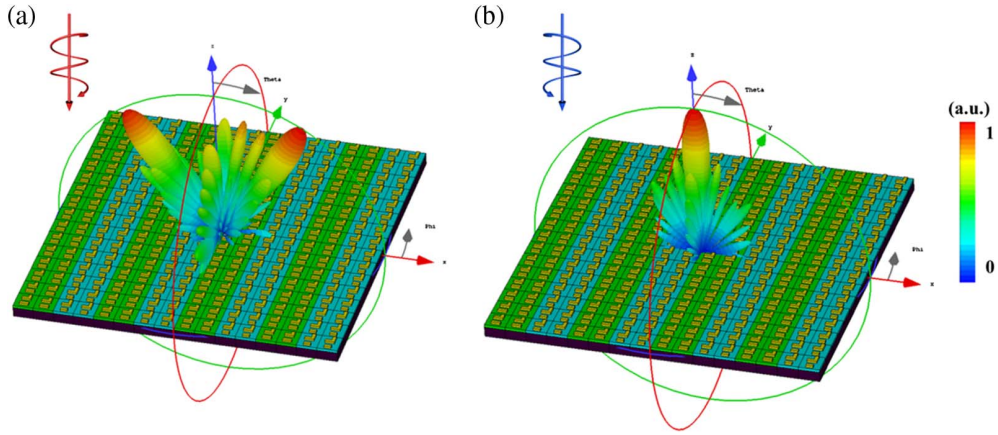

Fig. 7. Design of 1-bit coding metasurface based on ETP. Far-field scattering pattern of the coding metasurface under different incidences of (a) RCP and (b) LCP.

shown in red and indigo. To verify the feasibility of its encoding, a 1-bit encoded metasurface based on ETP was proposed. Two types of elements are arranged in the pattern of "0101," represented by green and blue colors, respectively. As mentioned earlier, these two elements exhibit a phase difference of π for RCP incidence, while they have the same phase for LCP incidence. Due to this feature, there is a significant difference in the reflected waves for different polarizations. Specifically, the reflected RCP waves are split and deflected in the $\pm 45°$ direction, while the reflected LCP waves are emitted vertically, as shown in Figs. 7(a) and 7(b). It is worth mentioning that the far-field scattering patterns here are all cross-polarized reflections. This polarization-selective characteristic is a result of the ETP. Compared to conventional phase coding metasurface that requires independent control of CP, the novel coding scheme based on the ETP greatly simplifies the design of metasurface structures and eliminates the need for complex phase calculations (see Appendix D).

In order to further explore the advantages of ET phase coding, we try to combine ETP with PB phase to design a compound phase coding metasurface to realize more complex CP beam modulation. Using the result of the ETP coding in the previous step, the "0" and "1" elements are both rotated 90° to achieve PB phase. A 2-bit compound phase coded metasurface

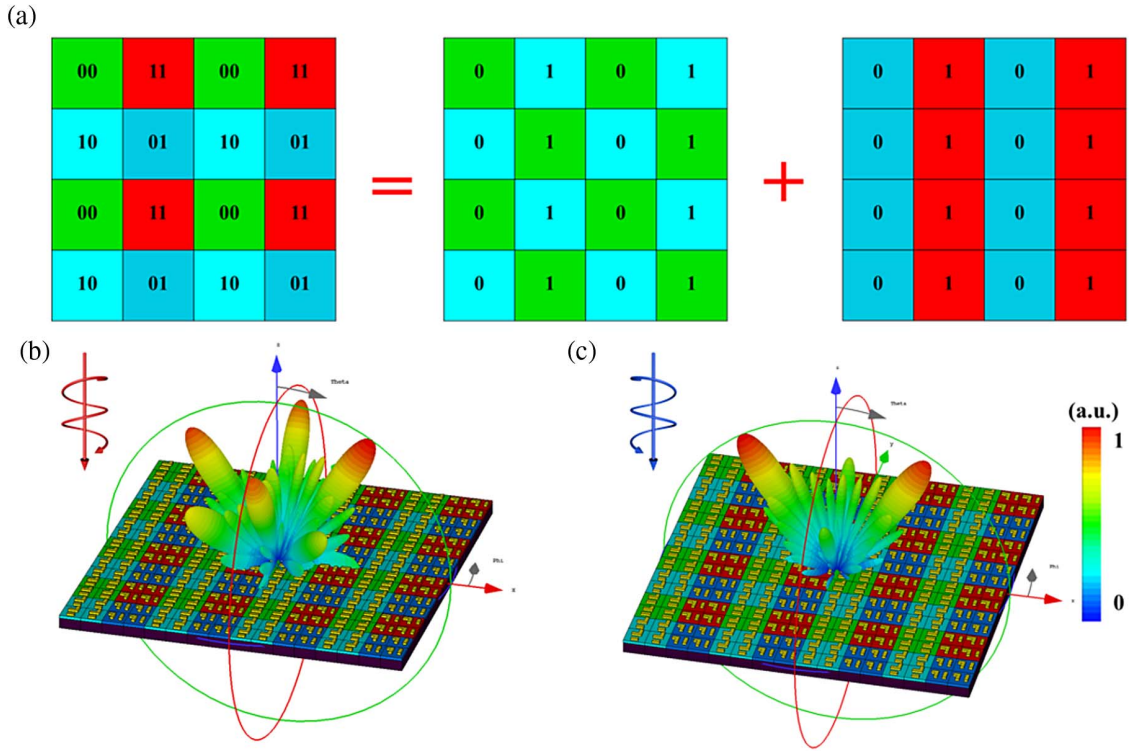

Fig. 8. Design of coding metasurface based on ETP and PB phase. (a) Schematic of the coding sequence. (b), (c) Far-field scattering pattern of the coding metasurface under different incidences of polarization.

is finally obtained through the convolution operation, as shown in Fig. 8. In fact, we still choose only "0" and "1" as two elements, but the rotation of the elements is increased. When RCP is incident, four-beam reflection is generated, while two-beam reflection corresponds to LCP incidence. When RCP is incident, the metasurface is 2-bit encoded due to the presence of EP. When LCP light is incident, the metasurface is equivalent to a 1-bit PB phase coded metasurface. The two designs can be in superposition since in contrast to the PB phase, the ETP is generated by circling a singularity and is topologically robust [28,37].

3. CONCLUSION

In a reflection regime, we have shown that a planar chiral plasmonic metasurface achieves 2π exceptional topological phase accumulation. It is demonstrated that only one of the circular polarization conversion beams, as specified by the chirality of the encircling exceptional point, is subject to 2π phase accumulation. By choosing two elements around an exceptional point, a coding metasurface can be realized based on exceptional topological phase and achieve the independent control of circular polarization. More importantly, exceptional topological phase can be combined with Pancharatnam-Berry phase to accomplish 2-bit coding metasurface designs. The 2π topological phase coding design based on the surrounding of an exceptional point is a new method in polarization control and extends the platform for nanophotonics applications by utilizing the nontrivial characteristics.

APPENDIX A: SIMULATED RESULTS OF THE REFLECTION SPECTRUM WITH LINEAR POLARIZATION INCIDENCE

In this section, we provide simulated data of the reflection spectrum in Fig. 9.

APPENDIX B: COUPLED-MODE THEORY

The metasurface consists of a nanostructure stacked with an anti "L" shaped rod and a straight rod in each meta-atom. The effective dipole moment of the structure is $p_{x,y} = \tilde{p}_{x,y}e^{i\omega t}$, which couples strongly to an incident radiation field $E_i = \tilde{E}_i e^{i\omega t}$ with a radiative coupling strength g_j. The resonant frequency and damping coefficient are ω_0 and γ, respectively. Assuming the incident radiation is close to the resonance ($\delta = \omega - \omega_0 \approx 0$) and damping is small ($\gamma \ll \omega_0$), the dipole moments of the nanostructure in the coupled system are related to the incident electric fields through the polarizability matrix as [27,28]

$$\begin{pmatrix} \delta_x + i\gamma_x + G_{xx} & G_{xy} \\ G_{yx} & \delta_y + i\gamma_y + G_{yy} \end{pmatrix} \begin{pmatrix} p_x \\ p_y \end{pmatrix} = \begin{pmatrix} g_x E_{ix} \\ g_y E_{iy} \end{pmatrix}, \tag{B1}$$

where the coupling term G_{jk} is a summation of the j-oriented radiation fields formed by the k-oriented dipole moments, which satisfies the condition $G_{xx} = G_{yy}$ due to the square lattice and $G_{xy} = G_{yx}$ due to the reciprocity. The reflected field by the dipole antenna array in the forward direction is

$$\begin{pmatrix} E_{rx} \\ E_{ry} \end{pmatrix} \equiv \hat{r} \begin{pmatrix} E_{ix} \\ E_{iy} \end{pmatrix} = \frac{i\omega\eta_0}{2a^2} \begin{pmatrix} p_x \\ p_y \end{pmatrix} - \begin{pmatrix} E_{ix} \\ E_{iy} \end{pmatrix}, \tag{B2}$$

where $\eta_0 = \sqrt{\mu_0/\varepsilon_0}$ is the impedance of vacuum, and a is the lattice constant of the metasurface. This passive system can be separated into an anisotropic PT symmetric part and a lossy isotropic part [27]:

$$\begin{pmatrix} -i\Gamma & G_{xy} \\ G_{xy} & i\Gamma \end{pmatrix} \begin{pmatrix} p_x \\ p_y \end{pmatrix} - S\overleftrightarrow{I} \begin{pmatrix} p_x \\ p_y \end{pmatrix} = \begin{pmatrix} g_x E_{ix} \\ g_y E_{iy} \end{pmatrix}, \tag{B3}$$

where $\Gamma = (\gamma_y - \gamma_x)/2$ and $S = \delta G_{xx} + i(\gamma_y - \gamma_x)/2$. The left part of Eq. (B2) can be thought of as a combination of a new matrix satisfying the PT symmetry and a background matrix with the same loss. However, the new matrix is PT symmetric and has the same eigenstates as the original matrix. This means that PT symmetry and EP can be achieved in our system. The corresponding Jones matrix for reflection is simply given by the superposition of the incident field and the field scattered by the dipole array in the forward direction. We can get the reflection matrix

$$\begin{pmatrix} E_{rx} \\ E_{ry} \end{pmatrix} = \left[A \begin{pmatrix} g_x^2(\delta_y + i\gamma_y + G_{yy}) & -g_x g_y G_{xy} \\ -g_x g_y G_{xy} & g_y^2(\delta_x + i\gamma_x + G_{xx}) \end{pmatrix} - \overleftrightarrow{I} \right] \times \begin{pmatrix} E_{ix} \\ \tilde{E}_{iy} \end{pmatrix}, \tag{B4}$$

where

$$A = \frac{i\omega\eta_0}{2a^2[(\delta_x + i\gamma_x + G_{xx})(\delta_y + i\gamma_y + G_{yy}) - G_{xy}^2]}. \tag{B5}$$

Combining Eqs. (B1) and (B2), we can rewrite the reflection matrix as

$$\begin{pmatrix} E_{rx} \\ E_{ry} \end{pmatrix} = (1 - g_x g_y AS)\overleftrightarrow{I} \begin{pmatrix} E_{ix} \\ E_{iy} \end{pmatrix} + g_x g_y A \begin{pmatrix} -i\Gamma & G_{xy} \\ G_{xy} & i\Gamma \end{pmatrix} \begin{pmatrix} E_{ix} \\ \tilde{E}_{iy} \end{pmatrix}. \tag{B6}$$

The eigenstates of the reflection matrix are the same as those of the matrix $\begin{pmatrix} -i\Gamma & G_{xy} \\ G_{xy} & i\Gamma \end{pmatrix}$. Thus, we can study the eigenvalue problems of the reflection matrix to reveal the EP and PT symmetry of the system.

APPENDIX C: COMBINATION WITH PANCHARATNAM-BERRY PHASE

Since ETP is a topological phase generated around a singularity, it can be combined with the PB phase to achieve independent encoding of RCP and LCP. Assuming that the metasurface is rotated at an angle of θ, the reflection matrix in the CP representation can be expressed as [38]

$$\hat{r}^{\theta}(\boldsymbol{R}) = \begin{pmatrix} r^{\theta}_{++}(\boldsymbol{R}) & r^{\theta}_{+-}(\boldsymbol{R}) \\ r^{\theta}_{-+}(\boldsymbol{R}) & r^{\theta}_{--}(\boldsymbol{R}) \end{pmatrix} = M(-\theta)\hat{r}(\boldsymbol{R})M(\theta). \tag{C1}$$

By employing the Pauli matrices notation $\{\sigma_1, \sigma_2, \sigma_3\}$ and the identity matrix $\overleftrightarrow{I}$, the matrix M is equal to $e^{i\theta\sigma_3}$, which can be expanded by Taylor series as $M(\theta) = \cos\theta\hat{I} + i\sin\theta\sigma_3$. The reflection matrix can be described as follows:

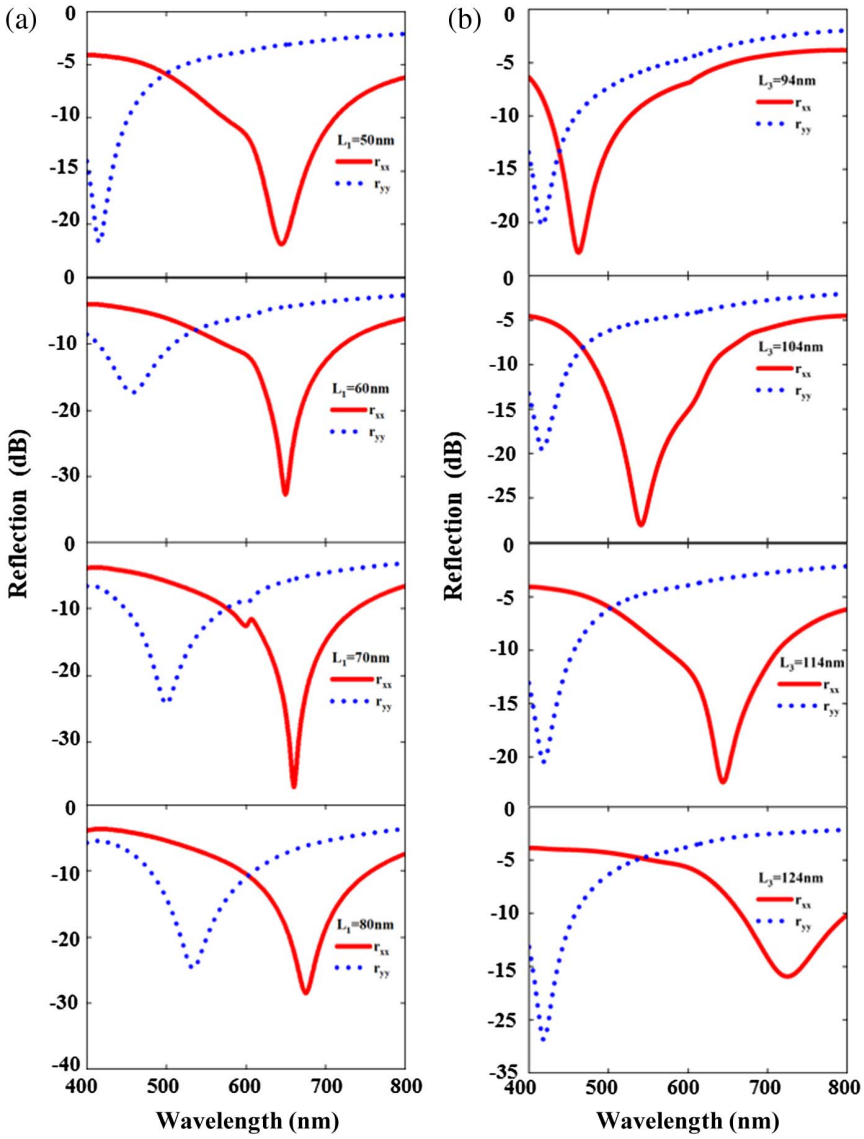

Fig. 9. (a) Simulated results with L_1 changed from 50 to 80 nm. The red and blue curves represent r_{xx} and r_{yy}, respectively. The effective length of the meta-atom in the y-direction is fixed, such that the resonance dips of r_{xx} keep constant. The effective length of the meta-atom in the x-direction is increasing, resulting in a red shift of the resonance dips of r_{yy}. (b) Simulated results with L_3 changed from 94 to 124 nm. The effective length of the meta-atom in the y-direction is fixed, such that the resonance dips of r_{yy} keep constant. The effective length of the meta-atom in the x-direction is increasing, resulting in a red shift of the resonance dips of r_{xx}. Therefore, by modulating the parameters of L_1 and L_3, orthogonal y- and x-polarized resonances can be degenerated, which means that the generation of EP is possible.

$$\hat{r}^{\theta}(\boldsymbol{R}) = \frac{1}{2}(r_{xx}+r_{yy})\hat{I} + \frac{i}{2}(r_{xy}-r_{yx})\sigma_3 + \frac{1}{2}(r_{xx}-r_{yy})(e^{-i2\theta}\sigma_+ + e^{i2\theta}\sigma_-) + \frac{i}{2}(r_{xy}+r_{yx})(-e^{-i2\theta}\sigma_+ + e^{i2\theta}\sigma_-). \quad \textbf{(C2)}$$

The + and − denote RCP and LCP light, respectively. Therefore, the cross-polarized reflection r^{θ}_{-+} can be described as

$$r^{\theta}_{-+}(\boldsymbol{R}) = \frac{(r_{xx}-r_{yy})+i(r_{xy}+r_{yx})}{2}e^{i2\theta} = r^{0}_{-+}(\boldsymbol{R})e^{i2\theta}, \quad \textbf{(C3)}$$

where r^{0}_{-+} represents the original ETP without rotation. Hence, a geometric phase of -2θ is applied to r_{-+} when the metasurface is rotated with an angle of θ. Similarly, the CP converted part r^{θ}_{+-} can be expressed as

$$r^{\theta}_{+-}(\boldsymbol{R}) = \frac{(r_{xx}-r_{yy})-i(r_{xy}+r_{yx})}{2}e^{-i2\theta} = r^{0}_{+-}(\boldsymbol{R})e^{-i2\theta}; \quad \textbf{(C4)}$$

thus, an opposite geometric phase of 2θ is applied to r_{+-}. In conclusion, the phase of CP conversion is

$$\varphi[r^{\theta}_{\pm\mp}(\boldsymbol{R})] = \varphi[r^{0}_{\pm\mp}(\boldsymbol{R})] \pm 2\theta. \quad \textbf{(C5)}$$

According to this, the combined original ETP with no rotation and a geometric phase makes up the overall phase of the CP conversion term with a rotation angle of θ.

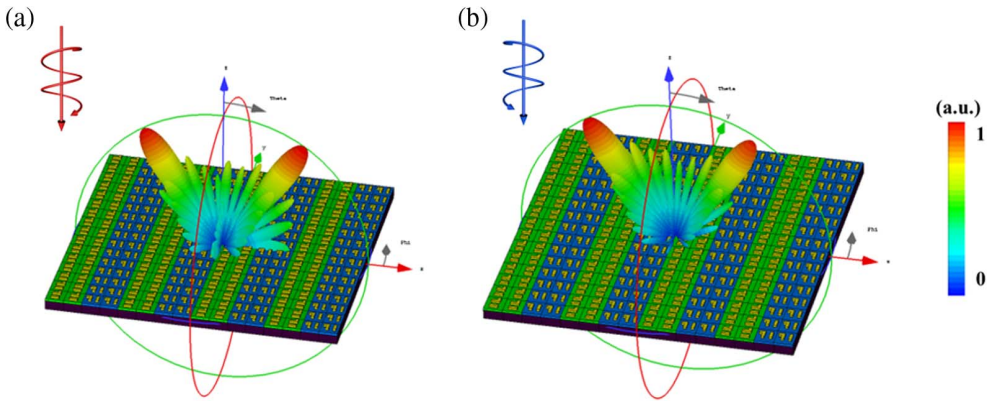

Fig. 10. Design of 1-bit coding metasurface based on Pancharatnam-Berry (PB) phase. The far-field scattering pattern of the coding metasurface under different incidences of (a) RCP and (b) LCP light. The parameters of the structure are $(L_1, L_3) = (81, 102)$ (nm); the "0" and "1" elements are encoded by rotating 90°. It reveals that they exhibit identical far-field scattering for various polarization incidences, which is essentially the result of the same coding method. The PB phase imparts different phase modulations for LCP and RCP light, with the same magnitude but opposite signs. Therefore, circularly polarized light cannot be controlled independently by the PB phase only.

APPENDIX D: LIMITATIONS OF PANCHARATNAM-BERRY PHASE CODING

In this section, we provide simulated data of the far-field scattering in Fig. 10.

Funding. National Natural Science Foundation of China (62175049, 62275061); Natural Science Foundation of Heilongjiang Province (ZD2020F002); Fundamental Research Funds for the Central Universities (3072022TS2509); Priority 2030 Federal Academic Leadership Program; Russian Science Foundation (23-72-10059).

Disclosures. The authors declare no conflicts of interest.

Data Availability. Data underlying the results presented in this paper are not publicly available at this time but may be obtained from the authors upon reasonable request.

REFERENCES

1. N. Yu, P. Genevet, M. A. Kats, *et al.*, "Light propagation with phase discontinuities: generalized laws of reflection and refraction," Science **334**, 333–337 (2011).
2. H.-T. Chen, A. J. Taylor, and N. Yu, "A review of metasurfaces: physics and applications," Rep. Prog. Phys. **79**, 076401 (2016).
3. S. B. Glybovski, S. A. Tretyakov, P. A. Belov, *et al.*, "Metasurfaces: from microwaves to visible," Phys. Rep. **634**, 1–72 (2016).
4. T. J. Cui, S. Liu, and L. Zhang, "Information metamaterials and metasurfaces," J. Mater. Chem. C **5**, 3644–3668 (2017).
5. A. S. Kupriianov, Y. Xu, A. Sayanskiy, *et al.*, "Metasurface engineering through bound states in the continuum," Phys. Rev. Appl. **12**, 014024 (2019).
6. S. Sun, Q. He, S. Xiao, *et al.*, "Gradient-index meta-surfaces as a bridge linking propagating waves and surface waves," Nat. Mater. **11**, 426–431 (2012).
7. L. Deng, J. Deng, Z. Guan, *et al.*, "Malus-metasurface-assisted polarization multiplexing," Light Sci. Appl. **9**, 101 (2020).
8. S. Zhang, P. Huo, W. Zhu, *et al.*, "Broadband detection of multiple spin and orbital angular momenta via dielectric metasurface," Laser Photonics Rev. **14**, 2000062 (2020).
9. L. Li, Z. Liu, X. Ren, *et al.*, "Metalens-array–based high-dimensional and multiphoton quantum source," Science **368**, 1487–1490 (2020).
10. Y. Bao, J. Yan, X. Yang, *et al.*, "Point-source geometric metasurface holography," Nano Lett. **21**, 2332–2338 (2021).
11. E. Minerbi, S. Keren-Zur, and T. Ellenbogen, "Nonlinear metasurface Fresnel zone plates for terahertz generation and manipulation," Nano Lett. **19**, 6072–6077 (2019).
12. T. J. Cui, M. Q. Qi, X. Wan, *et al.*, "Coding metamaterials, digital metamaterials and programmable metamaterials," Light Sci. Appl. **3**, e218 (2014).
13. S. Liu, T. J. Cui, Q. Xu, *et al.*, "Anisotropic coding metamaterials and their powerful manipulation of differently polarized terahertz waves," Light Sci. Appl. **5**, e16076 (2016).
14. L. Li, T. J. Cui, W. Ji, *et al.*, "Electromagnetic reprogrammable coding-metasurface holograms," Nat. Commun. **8**, 197 (2017).
15. J. Zhao, X. Yang, J. Y. Dai, *et al.*, "Programmable time-domain digital-coding metasurface for non-linear harmonic manipulation and new wireless communication systems," Natl. Sci. Rev. **6**, 231–238 (2019).
16. J. Han, X. Cao, J. Gao, *et al.*, "Broadband dual-circular polarized coding metasurfaces and their powerful manipulation of differently circular polarizations," Opt. Express **27**, 34141–34153 (2019).
17. C. Zheng, J. Li, G. Wang, *et al.*, "All-dielectric chiral coding metasurface based on spin-decoupling in terahertz band," Nanophotonics **10**, 1347–1355 (2021).
18. Y. Gou, H. F. Ma, L. W. Wu, *et al.*, "Non-interleaved polarization-frequency multiplexing metasurface for multichannel holography," Adv. Opt. Mater. **10**, 2201142 (2022).
19. J. P. Balthasar Mueller, N. A. Rubin, R. C. Devlin, *et al.*, "Metasurface polarization optics: independent phase control of arbitrary orthogonal states of polarization," Phys. Rev. Lett. **118**, 113901 (2017).
20. Y. Hu, L. Li, Y. Wang, *et al.*, "Trichromatic and tripolarization-channel holography with noninterleaved dielectric metasurface," Nano Lett. **20**, 994–1002 (2020).
21. R. Jin, L. Deng, L. Tang, *et al.*, "Decoupled phase modulation for circularly polarized light via chiral metasurfaces," ACS Photonics **10**, 155–161 (2023).
22. C. M. Bender and S. Boettcher, "Real spectra in non-Hermitian Hamiltonians having PT symmetry," Phys. Rev. Lett. **80**, 5243–5246 (1998).
23. C. Wang, W. R. Sweeney, A. D. Stone, *et al.*, "Coherent perfect absorption at an exceptional point," Science **373**, 1261–1265 (2021).
24. Q. Zhou, J. Wu, Z. Pu, *et al.*, "Observation of geometry-dependent skin effect in non-Hermitian phononic crystals with exceptional points," Nat. Commun. **14**, 4569 (2023).
25. J.-H. Park, A. Ndao, W. Cai, *et al.*, "Symmetry-breaking-induced plasmonic exceptional points and nanoscale sensing," Nat. Phys. **16**, 462–468 (2020).
26. W. He, Y. Hu, Z. Ren, *et al.*, "Transient loss-induced non-Hermitian degeneracies for ultrafast terahertz metadevices," Adv. Sci. **10**, 2304972 (2023).

27. M. Lawrence, N. Xu, X. Zhang, *et al.*, "Manifestation of PT symmetry breaking in polarization space with terahertz metasurfaces," Phys. Rev. Lett. **113**, 093901 (2014).
28. Q. Song, M. Odeh, J. Zúñiga-Pérez, *et al.*, "Plasmonic topological metasurface by encircling an exceptional point," Science **373**, 1133–1137 (2021).
29. X. Wu, J. Zhu, F. Lin, *et al.*, "Study of a high-index dielectric non-Hermitian metasurface and its application in holograms," ACS Omega **7**, 44743–44749 (2022).
30. S. Baek, S. H. Park, D. Oh, *et al.*, "Non-Hermitian chiral degeneracy of gated graphene metasurfaces," Light Sci. Appl. **12**, 87 (2023).
31. Y. Li, Z. Deng, C. Qin, *et al.*, "Bifunctional sensing based on an exceptional point with bilayer metasurfaces," Opt. Express **31**, 492–501 (2023).
32. P. Fu, S. Du, W. Lan, *et al.*, "Deep learning enabled topological design of exceptional points for multi-optical-parameter control," Commun. Phys. **6**, 254 (2023).
33. Y. Xu, L. Li, H. Jeong, *et al.*, "Subwavelength control of light transport at the exceptional point by non-Hermitian metagratings," Sci. Adv. **9**, eadf3510 (2023).
34. Z. Zhou, B. Jia, N. Wang, *et al.*, "Observation of perfectly-chiral exceptional point via bound state in the continuum," Phys. Rev. Lett. **130**, 116101 (2023).
35. A. D. Rakić, "Algorithm for the determination of intrinsic optical constants of metal films: application to aluminum," Appl. Opt. **34**, 4755–4767 (1995).
36. Ş. K. Özdemir, S. Rotter, F. Nori, *et al.*, "Parity–time symmetry and exceptional points in photonics," Nat. Mater. **18**, 783–798 (2019).
37. R. Colom, E. Mikheeva, K. Achouri, *et al.*, "Crossing of the branch cut: the topological origin of a universal 2π-phase retardation in non-Hermitian metasurfaces," Laser Photonics Rev. **17**, 2200976 (2023).
38. W. Luo, S. Xiao, Q. He, *et al.*, "Photonic spin Hall effect with nearly 100% efficiency," Adv. Opt. Mater. **3**, 1102–1108 (2015).